CHAPTER 6: ELECTROMAGNETICALLY RESTRAINED LITHIUM BLANKET

Contributors

Robert Woolley

6. ELECTROMAGNETICALLY RESTRAINED LITHIUM BLANKET

6.1 Introduction

This design concept would minimize fusion plant radioactivity for accidents or waste disposal, and also would provide other advantages. But whether the concept can be made to work at all is still uncertain.

To advance objectives of higher power density and reduced maintenance, thick liquid flowing walls blanket concepts eliminate solid plasma-facing materials and instead present a liquid free-surface directly to the plasma with no intervening solid material. A liquid has no crystal structure to be damaged by thermal stress or neutron bombardment. In the Electromagnetically Restrained (EMR) Lithium Blanket concept, an approximately one meter thick shell of liquid lithium metal almost completely surrounds a fusioning tokamak's toroidal plasma discharge, absorbing plasma particles, neutrons and other radiations while breeding tritium and collecting high temperature heat for power generation. The layer's thickness is chosen based on considerations of minimizing activation and damage to the solid chamber walls behind the liquid. The liquid lithium is flowing, and circulates in a loop through external equipment which removes chemically bound hydrogen isotopes, entrained helium, and high temperature heat. Of all possible liquid materials, pure lithium metal has the advantages of

a) high abundance,
b) superior tritium breeding,
c) low chemical toxicity, and
d) almost zero neutron activation.

Lithium's high chemical activity does require special care to avoid corrosion or fire. Lithium's high electrical conductivity may possibly permit efficient, compact MHD power generation. However, the high conductivity introduces challenges due to large MHD effects dominating the free-surface liquid metal flow.

The EMR concept strives to convert MHD difficulties introduced by the liquid metal's electrical conductivity into MHD advantages by deliberately injecting controlled electrical currents to influence liquid flow dynamics. A strong toroidal magnetic field is unavoidably present in the liquid lithium layer, since it is needed to confine the adjacent tokamak plasma. A force field is generated to push the liquid lithium against the chamber's walls by injecting current to flow through the liquid in the poloidal direction. The injected poloidal current interacts with the toroidal magnetic field to generate an internal "J X B" body force helping to keep the liquid lithium away from the plasma.

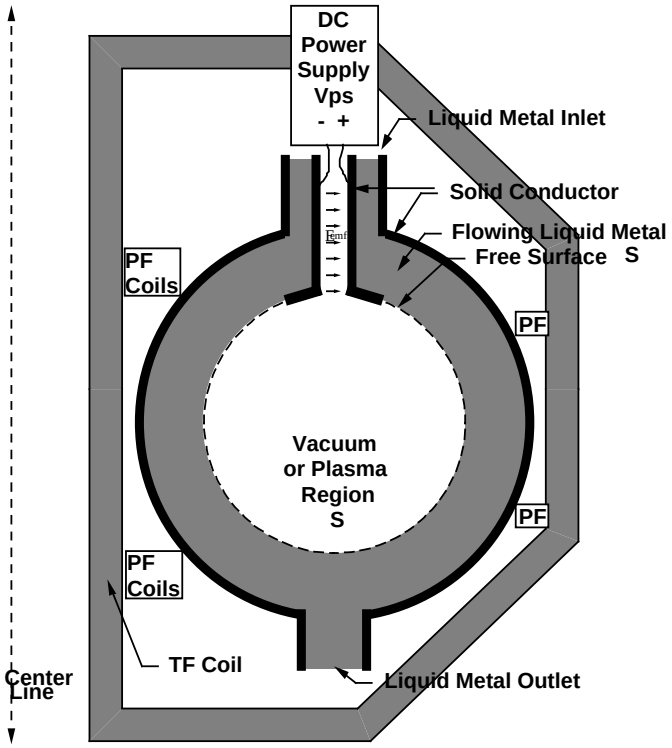

Figure 6.1: Electromagnetic Restraint (EMR) Lithium Blanket Concept

The electromagnetic forces developed within the liquid lithium are similar to the forces within a toroidal field coil magnet. Within a toroidal field coil, current flows in the poloidal direction through winding "turns", generating a magnetic field in the toroidal direction, The turn currents also interact with the toroidal magnetic field to produce a radial force on the turns, pushing the turns away from the enclosed toroidal volume. In the EMR Lithium Blanket concept, the lithium layer carries current in the same direction and sense as do the turns in the nearby toroidal field coils which enclose the plasma and blanket. The lithium layer thus acts like an additional toroidal field coil "turn" and is subject to typical TF coil turn forces.

Conducting liquids flowing across magnetic fields can generate large MHD forces opposing their motion, if a closed path exists for electric current to flow in response to their motion-induced electric field. For flow through pipes in a uniform magnetic field, the **U X B** electric field induced in the liquid metal by cross-field motion is not balanced by induced electric field in the stationary liquid adjacent to the pipe's wall, nor (if the pipe is conductive and not insulated) by any induced electric field in the stationary pipe wall itself. The resulting electric field imbalance drives circulating currents which interact with the magnetic field to oppose fluid motion, thus increasing pressure drop and the required pumping power. These MHD drag forces in pipes can be reduced somewhat by insulator coatings, but must be overcome by using high pumping pressure. On the other hand, for free-surface liquid flows which inherently have a low pressure gradient, external pumping

is not effective. The use of injected electric currents provides the possibility of compensating for some of the MHD effects in free-surface systems.

Some MHD effects can be avoided through axisymmetry and/or the electrically insulating nature of a free-surface. For instance axisymmetric vertical motion across a toroidal field produces a uniform radial electric field. If the liquid had an inner free-surface exposed to the vacuum (assumed insulating) then there would be no electrical currents or MHD drag pumping losses whatsoever, even with the outer liquid surface in direct contact with a conductive wall. And even if an inner wall were present there would still be no MHD drag if the two opposing walls were not electrically connected to each other.

The EMR concept is depicted in Figure 6.1. Two axisymmetric liquid lithium streams enter the toroidal chamber's top. The two streams are electrically separated there, either by an electrical insulator or by a noninsulating structure in which some electrical dissipation is wasted via leakage. At the top, the two streams are biased to different voltages via electrodes connected to an external power supply. Poloidal current injected via these electrodes is conducted through the streams which meet and join at the bottom of the chamber. The resulting **J X B** electromagnetic forces push the streams against the chamber walls and thus help hold them away from the plasma. The EMR Lithium Blanket concept makes use of these electromagnetic forces in conjunction with the other natural forces that exist, including centrifugal(inertial) forces, contact forces, viscosity, and surface tension.

In a variation on the EMR concept, a multi-pass design using sublayers also is envisioned. It would simultaneously achieve high exit temperature of the heated lithium while minimizing the maximum vapor pressure of the colder plasma-facing liquid lithium surface. Incoming streams at different temperatures would be combined to form sublayers in a special (TBD) injector nozzle at the chamber's entrance ports, and the exiting stream's sublayers would be mechanically separated in a special (TBD) diffuser apparatus at the chamber's exit ports. Relatively cold liquid introduced at the top of the chamber would form the plasma-facing free–surface sublayer. After flowing to the bottom, this partially heated exiting sublayer would be separated from the rest of the stream and pumped back to the top as the second stream. The second stream would be further heated by DT neutron interactions within the bulk fluid, and would exit at a hotter temperature than the plasma-facing free-surface. The sublayers scheme could stop here with two passes through the chamber, or additional passes could also be included. This EMR sublayer concept relies on the laminar characteristic of highly conductive free-surface liquid flows in a strong magnetic field, in which sublayers at different temperatures would thermally equilibrate only slowly via thermal conduction/diffusion, without turbulent convective mixing. The sublayer concept would not work in a poorly conductive and thus turbulent fluid such as FLiBe unless solid material separated the sublayers to prevent their mixing (as discussed in Section 7 for the CliFF concept). It may be permissable to enlist MHD effects to slow and thus thicken the sublayers heated solely by neutron reactions, since the high liquid speeds required by other thick liquid concepts to develop centrifugal force restraint may not be required in EMR schemes.

The known difficulty with the EMR concept is that the thick MHD liquid flow field is difficult to predict. Some feeling for this situation can be obtained by reviewing dimensionless parameters. The approximation in which magnetic induction is ignored could be valid for, e.g., a 2 m/s flow of a thin, 2 cm thick lithium layer, but would be completely wrong for a 1 meter thick, 10 m/s layer.. With lithium's 400°C electrical conductivity of $3.2*10^6$ S/m, a L=1 meter layer thickness and a u=10 m/s approximate speed, the Magnetic Reynolds Number is

$$Rm = \left\lfloor \frac{\text{Induced Magnetic Field}}{\text{Applied Magnetic Field}} \right\rfloor = \mu_0 \sigma \, \mathrm{u} L = 40$$

Thus, strong inductive MHD effects can easily dominate this flow regime. At the 5 Tesla magnetic field likely to be used in a reactor , the "Interaction Parameter" is

$$S = \left\lfloor \frac{\text{Passive EM Force Density}}{\text{Inertial Force Density}} \right\rfloor = \frac{\sigma}{\rho} \frac{{B_0}^2 L}{U} = 16000$$

and the Hartmann Number is

$$Ha = \sqrt{\frac{\text{Passive EM Force Density}}{\text{Viscous Force Density}}} = B_0 L \sqrt{\frac{\sigma}{\rho \nu}} = 4.6 * 10^5$$

Thus, strong MHD effects dominate all aspects of the flow regime.

The EMR concept has been investigated within APEX mainly as the part-time efforts of one person, due to the lack of design details for others to evaluate. The holdup has been the lack of tools to calculate flow fields for the EMR configuration. Therefore, the main focus has been the development of a computer simulation which includes without approximation all MHD phenomena needed to calculate flows for the EMR configuration. Simulation modeling is discussed in later sections below. (This simulation can be used to calculate flow fields for other concepts whose flow fields have already been approximately calculated by other codes.) At the end of the period covered by this APEX report, debugging of the computer simulation was still in progress, so no EMR flow configuration calculations had been completed. Therefore, no detailed engineering assessments of the EMR concept have been possible.

In addition to the analysis difficulties of predicting flows, it is possible that a useful flow field for this concept may not exist. Real MHD difficulties would be minimized by aligning the poloidal liquid metal flow velocity with both the injected poloidal current direction and with the poloidal flux surfaces of the plasma equilibrium. However, it is not possible to align these everywhere.

One troubling MHD phenomenon is the "diamagnetic drag" accompanying radial motion of liquid metal across the toroidal field, whose inherently inhomogeneous strength varies inversely with radius. Without requiring any interaction with stationary walls, the

radial motion induces a nonuniform vertical **u X B** electric field which in turn produces circulating closed loops of poloidal electrical current proportional to **curl(u X B)**, inherently associated with convecting toroidal magnetic flux between high and low field regions. These circulating current loops dissipate power, introduce fluid vorticity, and may substantially modify the J X B force profile in the liquid metal from that typical of a toroidal field coil "turn". If such radial motion across the toroidal field turns out to cause severe free-surface flow problems for the EMR concept, it may become necessary to investigate elongated plasma equilibria with low curvature for which radial motion of the free-surface liquid metal in the blanket can be kept small.

6.2 Comparison with other Thick Liquid Blanket Concepts

Other thick liquid blanket concepts differ in the material used but meet the same objectives regarding tritium breeding, absorbing most fusion power, and minimizing activation and damage to the solid chamber walls located behind the liquid. The two materials which have been considered by APEX are:

1.Tin-Lithium, a liquid tin and lithium mixture, and
2. FLiBe, a mixture of molten salts BeF_2 and LiF.

The Tin-Lithium material is highly conductive and dominated by MHD effects. The EMR concept could be applied directly to Tin-Lithium, and probably would be necessary in a thick liquid blanket to help counter MHD difficulties. The EMR flow details for Tin-Lithium would be more sensitive to centrifugal force and weight than flows for pure lithium since its mass density is far higher. The Tin-Lithium could be operated at a higher surface temperature based on its lower evaporation characteristics. A thinner layer of Tin-Lithium would suffice because of its better neutron moderating properties, but the tritium breeding ratio of Tin-Lithium is poorer than that for pure lithium. Tin-Lithium is less likely to burn in an accident than pure lithium, but Tin-Lithium is more of a radiological biohazard for accidents or for waste disposal. Tin is sufficiently abundant to not limit the future deployment of fusion power plants.

The thick liquid blanket concepts for FLiBe do not need to contend with dominant MHD effects. Their configurations are maintained via centrifugal inertial effects, which require high velocities, high mass flow rates, and high pumping power. FLiBe has a higher melting temperature than lithium and has different evaporation characteristics and different impurity effects on a plasma; it may have a smaller window of acceptable operating temperatures than pure lithium. FLiBe like pure lithium would not pose a radiological waste disposal hazard, but would be a radiological hazard for accident conditions. Like lithium, FLiBe is corrosive for many materials but unlike lithium, FliBe cannot burn. World resources of beryllium may limit the amount of FLiBe that can be produced, thus limiting the number of fusion plant blankets employing FLiBe which could be deployed.

The EMR Lithium Blanket may result in the lowest possible inventory of radioactive materials for all DT fusion power plant designs. It thus is appealing from a

radiological/safety point of view. Pure lithium is a near-zero activation material, with essentially zero activation in most circumstances. Its tritium breeding byproduct, helium, is inert for both nuclear and chemical reactions. Although its tritium breeding product is radioactive, tritium's only radiation is a low energy electron with no accompanying gamma rays. In a fusion reactor employing the EMR concept, the blanket should be continuously scrubbed of its bred tritium, resulting in a low tritium inventory susceptible to release in an accident. Bred tritium would be consumed in the plasma as it is produced. Lithium itself has no radioactive isotopes with significant half-lives. There is one "nearby" radioactive isotope of beryllium with a short half-life which beta decays with an accompanying gamma ray, but there are no single-step reactions capable of converting lithium to it, and multi-step reactions are not significant. This situation is in contrast to FLiBe which would contain products from nuclear reactions involving fluorine and beryllium, or tin-lithium which would include activated tin products. Whereas conventional blanket designs using a solid first wall typically includes a substantial amount of material which becomes radioactive due to neutron bombardment activation, the EMR concept has no first wall in front of the liquid to become activated. By designing the lithium layer to be sufficiently thick, activation of the wall behind the lithium can also be minimized. Thus, the EMR concept's only activated material results from neutron irradiation of the small unprotected solid plasma-facing material located between the two lithium streams' entrance ports.

From a chemical biological perspective, lithium is not especially toxic. Lithium compounds have even been administered as medication. This is in contrast to FliBe, considered a poison due to its Be content.

Lithium may improve the plasma performance Lithium is low-Z (after hydrogen and helium) and so is expected to have the smallest possible impact on plasma radiation losses, as compared to Fluorine and even higher Z elements. Some experience and theory suggest that lithium impurities may even improve plasma performance. It has been suggested that because of their complete absorption of incident hydrogen, lithium walls may end hydrogen recycling, leading to higher plasma edge temperature, better energy confinement, and improved fusion plasma performance. Lithium walls are expected to simplify vacuum pumping. Axisymmetric flowing liquid lithium walls are also expected to disallow penetration of nonaxisymmetric magnetic flux, and so may tend to oppose the growth of nonaxisymmetric magnetic islands in the plasma which can lead to disruptions.

Use of a single element, lithium, may simplify chemical processing of the blanket. This is in contrast to FLiBe, which is likely to develop various soluble impurities like hydrofluoric acid after some of the lithium and beryllium is consumed by neutron reactions.

6.3 Flow Phenomena with Injected Electric Current

Significant forces can be generated in liquid lithium metal without excessive electrical power. The threshold for significance may concern levitation. Lithium's mass density is about half of water's, so its gravitational weight density on Earth is about 5000

Newtons/m^3. With the approximately 5 Tesla toroidal field typical of many tokamak reactor designs, to generate a force field matching lithium's weight density requires a current density of $J=\rho g/B=1$ kA/m^2 in the lithium, which implies an electric field of 350 micro-volts/meter and an electric power dissipation of 0.35 watts/m^3. These are modest parameters. At this "one-gee" force-field level, a lithium EMR blanket surrounding an ITER-sized plasma would require a total current of 50 kA, implying a loop voltage of 0.01 volts, and a power of 500 watts. Increasing power to 1 MW would increase the lithium force field to the equivalent of 45 "gees".

On the other hand, the large value (>>1) of Rm, the Magnetic Reynolds Number, suggests the possibility of induced magnetic fields comperable to or stronger than the magnetic fields applied via the field coils, due to induced currents in the liquid lithium. Such induced currents would be stronger than any practical amount of injected electric current, would dissipate excessive power, and must be avoided. The design strategy for the EMR concept is to avoid excessive induced currents through choice of flow geometry.

6.4 Axisymmetric LMMHD Analyses

Although interest focuses on steady-state configurations, there is no reliable method for directly solving the highly nonlinear steady-state equations. Instead, a time-dependent simulation of the evolution of the configuration is developed. It will be used to find steady-state configurations by simulating the evolution of the MHD flow configuration until stops changing.

6.4.1 Review Of Equations For 3-D LMMHD With DC Power Supply

These general 3-D conventional equations following a standard development are first reviewed before formulating axisymmetric equations. We start with quasi-static electromagnetic field equations:

Ampere's Law:

$$\nabla \times \vec{B} = \mu \vec{J} \qquad (\Rightarrow \nabla \bullet \vec{J} = 0) \tag{1}$$

Faraday's Law:

$$\nabla \times \vec{E} = -\frac{\partial \vec{B}}{\partial t} \tag{2}$$

Divergence-Free Magnetic Fields

$$\nabla \bullet \vec{B} = 0 \tag{3}$$

Magnetic Vector Potential and Coulomb gauge

$$\nabla \times \vec{A} = \vec{B} \qquad \nabla \bullet \vec{A} = 0 \tag{4}$$

Substituting vector potential into Faraday's Law yields

$$\nabla \times \left(\vec{E} + \frac{\partial \vec{A}}{\partial t} \right) = 0 \;\Rightarrow\; \vec{E} = -\frac{\partial \vec{A}}{\partial t} - \nabla V \tag{5a,5b}$$

where V is voltage potential.

Ohm's Law:

$$\vec{J} = \sigma\left(\vec{E} + \vec{E}_{emf} + \vec{u} \times \vec{B}\right) \tag{6}$$

In Ohm's Law, the electromotive force (emf) of the electrical power supply has the mathematical form of a nonconservative electric field, which is nonzero only in the space between the power supply terminals, and is zero in the solid and liquid metal regions. Although electromotive force is not actually an electric field in the sense that it does not directly contribute to Faraday's law, it is used here to include power supply effects.

The vector field, $\vec{u}$, represents conductor velocity.

Combining the curl of Ohm's law with Faraday's law gives:

$$\frac{\partial \vec{B}}{\partial t} = \nabla \times \left(\vec{u} \times \vec{B}\right) - \nabla \times \frac{\vec{J}}{\sigma} + \nabla \times \vec{E}_{emf} \tag{7}$$

Eliminate current density via Eq. (1) and invoke Eq. (3), and the result is

$$\frac{\partial \vec{B}}{\partial t} = \nabla \times (\vec{u} \times \vec{B}) + \frac{1}{\sigma\mu} \vec{\nabla}^2 \vec{B} + \nabla \times \vec{E}_{emf} \tag{8}$$

Motion of the liquid metal is modeled by the Navier-Stokes equations for incompressible flow with constant properties (e.g. density and viscosity), with body forces including gravity and electromagnetism, and with surface tension effects acting on the free surface. In vector form, ,

$$\nabla \bullet \vec{u} = 0 \tag{9}$$

$$\frac{\partial \vec{u}}{\partial t} + (\vec{u} \bullet \nabla)\vec{u} = -\frac{\nabla p}{\rho} + \nu \vec{\nabla}^2 \vec{u} + \vec{g} + \frac{\vec{J} \times \vec{B}}{\rho} \qquad (10)$$

where $\vec{g} = g_z \hat{a}_z$ with g_z=-9.8 m/s^2 on the earth's surface.

The equations for 3-D LMMHD with a power supply are thus (3), (8), (9), and (10). They need to be joined with suitable boundary conditions for pressure p, magnetic field, and velocity.

It should be mentioned that there is a subtlety in using Equation (8) directly in a simulation. Equation (8) expresses the time derivative of magnetic field at a point as a function of spatial derivatives at that same location only, independent of values at other locations. It may seem paradoxical that in the case of two nested toroidal solenoid coil windings, a time varying current in the inner winding induces a time-varying voltage in the outer winding even though it produces identically zero magnetic field at the outer winding location. The difficulty can be attributed to the non local requirements imposed by Stokes' Theorem on contour integrals of fields whose curl appears in the equations. Because the vector potential, $\vec{A}$, does not vanish outside a solenoid despite the fact that $\vec{B} = \nabla \times \vec{A}$ does, computer calculations using $\vec{A}$ as a field variable instead of $\vec{B}$ are conventional practice for time-varying magnetic situations such as those involving eddy currents. The joint computation of spatially continuous $\vec{B}$ and $\vec{E}$ fields for simply connected computational domains is another approach which should work correctly for time varying situations.

6.4.2 Derivation Of Axisymmetric LMMHD Equations

Use of toroidally continuous axisymetric liquid metal flows can reduce MHD drag effects as noted earlier. But there are also other reasons to enforce axisymmetry near the plasma. If highly conductive liquid metal were flowing in nonaxisymmetic patterns beside a tokamak plasma, MHD effects would produce nonaxisymmetric currents in the liquid, which in turn would produce nonaxisymmetric magnetic fields to perturb the plasma. Tokamaks and several other plasma confinement schemes require precisely axisymmetric magnetic fields to maintain nested internal flux surfaces. They have low tolerance for departures from axisymmetry and develop "magnetic islands" which deteriorate plasma confinement at very small levels of nonaxisymmetric magnetic field "ripple". A reactor blanket should avoid doing harm to the plasma equilibrium, so axisymmetry is an important requirement for the near-plasma portions of a highly conductive, fast moving, liquid blanket. Thus, all simulation variables are modeled as having axisymmetric geometry, as is appropriate for LMMHD designs intended to operate in close proximity to the necessarily axisymmetric tokamak plasma's magnetic confinement geometry.

Although exact 3-D MHD equations for an incompressible liquid are complicated, they are substantially simplified without approximation by the requirement for axisymmetry. The fundamental simulation variables have been chosen in a novel manner which avoids

any need to numerically integrate electromagnetic partial differential equations through vacuum regions, instead relying on analytical expressions to give boundary conditions on conducting material surfaces. The simulated electrical variables which do vary within conducting regions are the poloidal threading current and the poloidal magnetic flux.

In deriving exact axisymmetric LMMHD equations with independent variables (r,z,t), it is convenient to express magnetic field via poloidal magnetic flux stream function, Ψ, and the total poloidal threading current stream function, I (including any Toroidal Field coil system current). One could also employ a velocity stream function and vorticity formulation, but that does not appear to simplify the equations.)

The axisymmetric time-varying vector field variables to be computed are the fluid velocity , $\vec{u}$, and the magnetic field, $\vec{B}$, represented in cylindrical component form as

$$\vec{u} = u_r \hat{a}_r + u_\varphi \hat{\varphi} + u_z \hat{a}_z$$
$$\vec{B} = B_r \hat{a}_r + B_\varphi \hat{\varphi} + B_z \hat{a}_z \qquad (11a,11b)$$

Axisymmetry requires that $\frac{\partial}{\partial \varphi}(\bullet) = 0$ for every variable, and simplifies differential operator forms.

Because of axisymmetry, the toroidal field in a vacuum region varies as

$$B_\varphi = \frac{B_0 R_0}{r} \qquad (12)$$

for some value of B_0R_0. In a tokamak plasma the externally imposed toroidal field is typically much stronger than the variations in toroidal field caused by poloidal plasma currents, so the toroidal field still varies approximately as given by Equation (12) even when a tokamak plasma is present. As depicted in Figure 1, the contour ∂S lies in a poloidal plane and surrounds only the vacuum (i.e., plasma) region which is enclosed inside the metallic conducting region. Using Equation (12) to calculate the enclosed toroidal field magnetic flux gives:

$$\Phi = \int_S \frac{B_0 R_0}{r} dr\, dz = B_0 R_0 \oint_{\partial S} \frac{z}{r} dr \qquad (13)$$

where the integral around the Figure 1 contour, ?S, is evaluated in the clockwise direction as per Stokes' theorem. This enclosed toroidal magnetic flux variable, Φ, cannot change instantaneously because it is surrounded by conducting material. It thus is an appropriate choice to use directly as a dynamic simulation state variable. Integrating the toroidal component of Equation (7) over the Figure 1 vacuum region, S, and invoking Stoke's theorem gives its time rate of change vs. the power supply voltage and other variables:

$$\frac{\partial \Phi}{\partial t} = V_{PS} - \oint_{\partial S} \frac{\vec{J}}{\sigma} \bullet d\vec{\ell} + \oint_{\partial S} \vec{u} \times \vec{B} \bullet d\vec{\ell} \qquad (14)$$

In axisymmetric geometry, the total net poloidal "threading current" between the center line axis of symmetry and any (r,z) location, expressed in ampere-turns, is related to the local toroidal field, $B_?(r,z)$, by

$$I(r,z) = \frac{2\pi}{\mu} r B_{\varphi}(r,z) \qquad (15)$$

In particular, a single constant value of this threading current, I_s is valid for all locations throughout the enclosed vacuum region and its boundary:

$$I_s = \frac{2\pi}{\mu} B_0 R_0 \qquad (16)$$

Combining these equations gives the poloidal threading current's boundary condition value on the enclosed liquid metal-vacuum interface, in terms of the trapped toroidal flux, ?, and the boundary's shape:

$$I_s = \frac{2\pi}{\mu} \frac{\Phi}{\oint_{\partial S} \frac{z}{r} dr} \qquad (17)$$

The other spatially constant boundary condition value of poloidal threading current is on the exterior surface of the conducting region. It is simply the toroidal field coil system's total ampere-turns, I_{TF}. which is assumed to remain constant in time.

The conducting region includes a flowing liquid metal subregion and a solid metal backing subregion. Within each subregion the simulation models the metal conductivity, σ, as a constant value, with different values in different subregions. The boundary condition at the solid/liquid interface requires continuity of the tangential electric field and of the normal current density:

$$\left[\begin{matrix} \left(\frac{n_r}{\sigma}\right) & \left(\frac{n_z}{\sigma}\right) \\ n_z & -n_r \end{matrix}\right] \left[\begin{matrix} \frac{\partial I}{\partial r} \\ \frac{\partial I}{\partial z} \end{matrix}\right]_{Liquid} = \left[\begin{matrix} \left(\frac{n_r}{\sigma}\right) & \left(\frac{n_z}{\sigma}\right) \\ n_z & -n_r \end{matrix}\right] \left[\begin{matrix} \frac{\partial I}{\partial r} \\ \frac{\partial I}{\partial z} \end{matrix}\right]_{Solid} \qquad (18)$$

Here, (n_r, n_z) is a unit vector perpendicular to the solid/liquid interface.

The poloidal current density can be expressed in terms of the "threading current", as

$$\vec{J}_P = J_r\hat{a}_r + J_z\hat{a}_z = \nabla\times\left(\frac{I\hat{\varphi}}{2\pi r}\right) \tag{19}$$

or in component form,

$$J_r = -\frac{1}{2\pi r}\frac{\partial I}{\partial z} \qquad J_z = +\frac{1}{2\pi r}\frac{\partial I}{\partial r} \tag{20a,b}$$

which allows the contour integral involving current density to be rewritten as

$$\oint_{\partial S}\frac{\vec{J}}{\sigma}\bullet d\vec{\ell} = \frac{1}{\sigma}\oint_{\partial S}\left(\nabla\times\left(\frac{I\hat{\varphi}}{2\pi r}\right)\right)\bullet d\vec{\ell} = \frac{1}{2\pi\sigma}\oint_{\partial S}\left(\frac{\partial I}{\partial r}\frac{dz}{r} - \frac{\partial I}{\partial z}\frac{dr}{r}\right) \tag{21}$$

Using Equation (15) for the toroidal field component, the other contour integral in Equation (14) can be rewritten as

$$\oint_{\partial S}\vec{u}\times\vec{B}\bullet d\vec{\ell} = \oint_{\partial S}(u_r\hat{a}_r + u_\varphi\hat{\varphi} + u_z\hat{a}_z)\times(B_r\hat{a}_r + \frac{\mu I}{2\pi r}\hat{\varphi} + B_z\hat{a}_z)\bullet(\hat{a}_r dr + \hat{a}_z dz) = \oint_{\partial S}\frac{\mu I}{2\pi r}(u_r dz - u_z dr) + \oint_{\partial S}u_\varphi(B_z dr - B_r dz) \tag{22}$$

We can also define ?, as the net poloidal magnetic flux between the center line axis of symmetry and any (r,z) location. Then the poloidal field can be written as:

$$\vec{B}_P = B_r\hat{a}_r + B_z\hat{a}_z = \nabla\times\left(\frac{\Psi\hat{\varphi}}{2\pi r}\right) \tag{23}$$

or in component form, as

$$B_r = -\frac{1}{2\pi r}\frac{\partial\Psi}{\partial z} \qquad B_z = +\frac{1}{2\pi r}\frac{\partial\Psi}{\partial r} \tag{24a,b}$$

Then the final integral in equation (22) can be rewritten as

$$\oint_{\partial S} u_\varphi (B_z dr - B_r dz) = \frac{1}{2\pi}\oint_{\partial S} \frac{u_\varphi}{r}\left(\frac{\partial \Psi}{\partial r}dr + \frac{\partial \Psi}{\partial z}dz\right) = \frac{1}{2\pi}\oint_{\partial S}\frac{u_\varphi}{r}d\Psi \tag{25}$$

Combining equations (21), (22) and (25) with (14) results in:

$$\frac{d\Phi}{dt} = V_{PS} - \frac{1}{2\pi\sigma}\oint_{\partial S}\left(\frac{\partial I}{\partial r}\frac{\partial z}{r} - \frac{\partial I}{\partial z}\frac{\partial r}{r}\right) + \frac{\mu I_s}{2\pi}\oint_{\partial S}\frac{(u_r dz - u_z dr)}{r} + \frac{1}{2\pi}\oint_{\partial S}\frac{u_\varphi}{r}d\Psi \tag{26}$$

Since E_{emf}=0 in the conducting region, the field dynamics there are obtained from Equation (7) and Ampere's law, as:

$$\frac{\partial \vec{B}}{\partial t} = \nabla \times \left(\vec{u} \times \vec{B}\right) + \frac{1}{\sigma\mu}\vec{\nabla}^2\vec{B} \tag{27}$$

Fixing attention on the toroidal components,

$$\frac{\partial B_\varphi}{\partial t} = \hat{\varphi} \bullet \left(\nabla \times \left(\vec{u} \times \vec{B}\right)\right) + \hat{\varphi} \bullet \left(\frac{1}{\sigma\mu}\vec{\nabla}^2\vec{B}\right) \tag{28}$$

shows the dissipative term is completely independent of the poloidal field,

$$\hat{\varphi} \bullet \vec{\nabla}^2\vec{B} = \frac{1}{r}\frac{\partial}{\partial r}\left(r\frac{\partial B_\varphi}{\partial r}\right) + \frac{\partial^2 B_\varphi}{\partial r^2} - \frac{B_\varphi}{r^2} \tag{29}$$

and may be rewritten in terms of the poloidal threading current as:

$$\hat{\varphi} \bullet \vec{\nabla}^2\vec{B} = \frac{\mu}{2\pi}\left(\frac{1}{r}\frac{\partial}{\partial r}\left(r\frac{\partial}{\partial r}\left(\frac{I}{r}\right)\right) + \frac{\partial^2}{\partial z^2}\left(\frac{I}{r}\right) - \frac{1}{r^2}\left(\frac{I}{r}\right)\right) = \frac{\mu}{2\pi r}\Delta^* I \tag{30}$$

where Δ^* is the Grad-Shafranov operator,

$$\Delta^* := r\frac{\partial}{\partial r}\frac{1}{r}\frac{\partial}{\partial r} + \frac{\partial^2}{\partial z^2} \tag{31}$$

Thus the substitution of Equation (30) into Equation (28) gives:

$$\frac{\partial I(r,z,t)}{\partial t} = \frac{1}{\sigma\mu}\Delta^* I(r,z,t) + \frac{2\pi r}{\mu}\hat{\varphi}\bullet\left(\nabla\times\left(\vec{u}\times\vec{B}\right)\right) \tag{32}$$

The last term of Equation (32) can be rewritten in terms of the components, as

$$\begin{aligned}\frac{2\pi r}{\mu}\hat{\varphi}\bullet(\nabla\times(\vec{u}\times\vec{B})) &= -r\left(\frac{\partial}{\partial r}\left(\frac{u_r I}{r}\right)+\frac{\partial}{\partial z}\left(\frac{u_z I}{r}\right)\right)+\frac{2\pi r}{\mu}\left(\frac{\partial}{\partial r}(u_\varphi B_r)+\frac{\partial}{\partial z}(u_\varphi B_z)\right)\\ &= r\left(-\frac{u_z}{r}\frac{\partial I}{\partial z}-\frac{u_r}{r}\frac{\partial I}{\partial r}+\frac{u_r I}{r^2}-\frac{I}{r}\left(\frac{\partial u_r}{\partial r}+\frac{\partial u_z}{\partial z}\right)\right)+\frac{r}{\mu}\left(\frac{\partial}{\partial r}\left(\frac{u_\varphi}{r}\left(-\frac{\partial\Psi}{\partial z}\right)\right)+\frac{\partial}{\partial z}\left(\frac{u_\varphi}{r}\frac{\partial\Psi}{\partial r}\right)\right)\\ &= -u_r\frac{\partial I}{\partial r}-u_z\frac{\partial I}{\partial z}+\frac{2u_r I}{r}+\frac{r}{\mu}\left(\frac{\partial\Psi}{\partial r}\frac{\partial}{\partial z}\left(\frac{u_\varphi}{r}\right)-\frac{\partial\Psi}{\partial z}\frac{\partial}{\partial r}\left(\frac{u_\varphi}{r}\right)\right)\end{aligned} \tag{33}$$

The last terms in Equation (33) can be rewritten as a cross product of gradients:

$$\frac{r}{\mu}\left(\frac{\partial\Psi}{\partial r}\frac{\partial}{\partial z}\left(\frac{u_\varphi}{r}\right)-\frac{\partial\Psi}{\partial z}\frac{\partial}{\partial r}\left(\frac{u_\varphi}{r}\right)\right)=\frac{r}{\mu}(\nabla\Psi)\times\nabla\left(\frac{u_\varphi}{r}\right) \tag{34}$$

Substituting Equations (33) and (34) into (32) gives the evolution equation for the poloidal threading current variable:

$$\frac{\partial I}{\partial t} = -u_r\frac{\partial I}{\partial r}-u_z\frac{\partial I}{\partial z}+\frac{1}{\sigma\mu}\Delta^* I+\frac{2u_r I}{r}+\frac{r}{\mu}\nabla\Psi\times\nabla\left(\frac{u_\varphi}{r}\right) \tag{35}$$

For the liquid motion equations (9) and (10), there is a “no-slip” boundary condition specifying the liquid velocity on all stationary material surfaces,

$$\vec{u}(\bullet,t)\big|_{\text{MaterialSurface}} = 0 \tag{36}$$

The pressure “boundary condition” on the free surface is

$$p\big|_{\text{FreeSurface}} = \gamma\left(\frac{1}{R_1}+\frac{1}{R2}\right) \tag{37}$$

where R_1 and R_2 are the surface’s local radii of curvature and the surface tension parameter, γ, is a material constant.

The electromagnetic force can be resolved into cylindrical components as follows:

$$\begin{aligned}\vec{J}\times\vec{B} &= [-\frac{1}{2\pi r}\frac{\partial I}{\partial z}\hat{a}_r + J_\varphi\hat{\varphi} + \frac{1}{2\pi r}\frac{\partial I}{\partial r}\hat{a}_z]\times[B_r\hat{a}_r + \frac{\mu I}{2\pi r}\hat{\varphi} + B_z\hat{a}_z] \\ &= \{J_\varphi B_z - (\frac{1}{2\pi r}\frac{\partial I}{\partial r})(\frac{\mu I}{2\pi r})\}\hat{a}_r \\ &\quad + \{(\frac{1}{2\pi r}\frac{\partial I}{\partial r})B_r - (-\frac{1}{2\pi r}\frac{\partial I}{\partial z})B_z\}\hat{\varphi} \\ &\quad + \{(-\frac{1}{2\pi r}\frac{\partial I}{\partial z})(\frac{\mu I}{2\pi r}) - B_r J_\varphi\}\hat{a}_z\end{aligned} \tag{38}$$

Then the continuity (9) and Navier-Stokes (10) axisymmetric equations can be written in cylindrical coordinates component form as follows:

$$\frac{1}{r}\frac{\partial(ru_r)}{\partial r} + \frac{\partial u_z}{\partial z} = 0 \tag{39}$$

$$\begin{aligned}\frac{\partial u_r}{\partial t} &= \frac{u_\varphi^2}{r} - u_r\frac{\partial u_r}{\partial r} - u_z\frac{\partial u_r}{\partial z} - \frac{1}{\rho}\frac{\partial p}{\partial r} + \nu(\frac{1}{r}\frac{\partial}{\partial r}(r\frac{\partial u_r}{\partial r}) + \frac{\partial^2 u_r}{\partial z^2} - \frac{u_r}{r^2}) \\ &\quad + \frac{J_\varphi B_z}{\rho} - \frac{\mu I}{4\pi^2 r^2\rho}\frac{\partial I}{\partial r}\end{aligned} \tag{40}$$

$$\begin{aligned}\frac{\partial u_\varphi}{\partial t} &= -\frac{u_r u_\varphi}{r} - u_r\frac{\partial u_\varphi}{\partial r} - u_z\frac{\partial u_\varphi}{\partial z} + \nu(\frac{1}{r}\frac{\partial}{\partial r}(r\frac{\partial u_\varphi}{\partial r}) + \frac{\partial^2 u_\varphi}{\partial z^2} - \frac{u_\varphi}{r^2}) \\ &\quad + \frac{1}{2\pi r\rho}(\frac{\partial I}{\partial r}B_r + \frac{\partial I}{\partial z}B_z\}\end{aligned} \tag{41}$$

$$\begin{aligned}\frac{\partial u_z}{\partial t} &= -u_r\frac{\partial u_z}{\partial r} - u_z\frac{\partial u_z}{\partial z} - \frac{1}{\rho}\frac{\partial p}{\partial z} + \nu(\frac{1}{r}\frac{\partial}{\partial r}(r\frac{\partial u_z}{\partial r}) + \frac{\partial^2 u_z}{\partial z^2}) \\ &\quad + g_z - \frac{J_\varphi B_r}{\rho} - \frac{\mu I}{4\pi^2 r^2\rho}\frac{\partial I}{\partial z}\end{aligned} \tag{42}$$

However, the toroidal component of current is related to the poloidal flux via

$$\begin{aligned}\mu J_\varphi\hat{\varphi} &= \nabla\times\vec{B}_P \\ &= \nabla\times(\nabla\times(\frac{\Psi\hat{\varphi}}{2\pi r})) \\ &= -\vec{\nabla}^2(\frac{\Psi\hat{\varphi}}{2\pi r})\end{aligned}$$

so that

$$J_\varphi = -\frac{1}{2\pi r\mu}\Delta^*\Psi \qquad \text{where} \quad \Delta^* := r\frac{\partial}{\partial r}\frac{1}{r}\frac{\partial}{\partial r} + \frac{\partial^2}{\partial z^2} \quad \text{is the Grad-Shafranov operator, again.}$$

Thus the velocity evolution equations become:

$$\frac{\partial u_r}{\partial t} = \frac{u_\varphi^2}{r} - u_r\frac{\partial u_r}{\partial r} - u_z\frac{\partial u_r}{\partial z} - \frac{1}{\rho}\frac{\partial p}{\partial r} + \nu\left(\frac{1}{r}\frac{\partial}{\partial r}\left(r\frac{\partial u_r}{\partial r}\right) + \frac{\partial^2 u_r}{\partial z^2} - \frac{u_r}{r^2}\right) - \frac{\Delta^*\Psi}{4\pi^2 r^2\rho\mu}\frac{\partial\Psi}{\partial r} - \frac{\mu I}{4\pi^2 r^2\rho}\frac{\partial I}{\partial r} \tag{43}$$

$$\frac{\partial u_\varphi}{\partial t} = -\frac{u_r u_\varphi}{r} - u_r\frac{\partial u_\varphi}{\partial r} - u_z\frac{\partial u_\varphi}{\partial z} + \nu\left(\frac{1}{r}\frac{\partial}{\partial r}\left(r\frac{\partial u_\varphi}{\partial r}\right) + \frac{\partial^2 u_\varphi}{\partial z^2} - \frac{u_\varphi}{r^2}\right) + \frac{1}{4\pi^2 r^2\rho}\left(\frac{\partial I}{\partial z}\frac{\partial\Psi}{\partial r} - \frac{\partial I}{\partial r}\frac{\partial\Psi}{\partial z}\right\} \tag{44}$$

$$\frac{\partial u_z}{\partial t} = -u_r\frac{\partial u_z}{\partial r} - u_z\frac{\partial u_z}{\partial z} - \frac{1}{\rho}\frac{\partial p}{\partial z} + \nu\left(\frac{1}{r}\frac{\partial}{\partial r}\left(r\frac{\partial u_z}{\partial r}\right) + \frac{\partial^2 u_z}{\partial z^2}\right) + g_z - \frac{\Delta^*\Psi}{4\pi^2 r^2\rho\mu}\frac{\partial\Psi}{\partial z} - \frac{\mu I}{4\pi^2 r^2\rho}\frac{\partial I}{\partial z} \tag{45}$$

In order to enforce the divergence-free velocity condition, the pressure field must in general have a particular non-zero divergence . Taking the divergence of Equation (34) and requiring that $\nabla\bullet\vec{u} = 0 \Rightarrow \nabla\bullet\frac{\partial\vec{u}}{\partial t} = 0$, we get the Pressure Poisson Equation:

$$\nabla^2 p = -\rho\nabla\bullet[(\vec{u}\bullet\nabla)\vec{u}] + \nabla\bullet(\vec{J}\times\vec{B}) \tag{46}$$

where spatially constant density and kinematic viscosity have been assumed. In component form this can be rewritten as:

$$\nabla^2 p = -\rho\left(\frac{1}{r}\frac{\partial}{\partial r}\left(r\left[\frac{u_\varphi^2}{r} - u_r\frac{\partial u_r}{\partial r} - u_z\frac{\partial u_r}{\partial z}\right]\right) + \frac{\partial}{\partial z}\left[-u_r\frac{\partial u_z}{\partial r} - u_z\frac{\partial u_z}{\partial z}\right]\right) - \frac{1}{4\pi^2 r\rho}\left(\frac{\partial}{\partial r}\left(\frac{1}{r}\left[\frac{\Delta^*\Psi}{\mu}\frac{\partial\Psi}{\partial r} + \mu I\frac{\partial I}{\partial r}\right]\right) + \frac{\partial}{\partial z}\left(\frac{1}{r}\left[\frac{\Delta^*\Psi}{\mu}\frac{\partial\Psi}{\partial z} + \mu I\frac{\partial I}{\partial z}\right]\right)\right) \tag{47}$$

The evolution equation for poloidal flux is obtained by substituting Equations (21) and (42) into (24) and combining terms:

$$\frac{\partial \Psi}{\partial t} = -u_r \frac{\partial \Psi}{\partial r} - u_z \frac{\partial \Psi}{\partial z} + \frac{1}{\sigma \mu} \Delta^* \Psi \tag{48}$$

Boundary conditions for poloidal flux are implemented via the MacDonald-Wexler algorithm, which uses Greens functions related to the finite region boundary.

6.4.3 Summary Of Simulation Equations

The following scalar equations define the EMR configuration to be simulated:

$$\frac{\partial I}{\partial t} = -u_r \frac{\partial I}{\partial r} - u_z \frac{\partial I}{\partial z} + \frac{1}{\sigma\mu}\Delta^* I + \frac{2u_r I}{r} + \frac{r}{\mu}\nabla\Psi \times \nabla\left(\frac{u_\varphi}{r}\right) \tag{S1}$$

$$\frac{\partial \Psi}{\partial t} = -u_r \frac{\partial \Psi}{\partial r} - u_z \frac{\partial \Psi}{\partial z} + \frac{1}{\sigma\mu}\Delta^* \Psi \tag{S2}$$

$$\frac{\partial u_r}{\partial t} = \frac{u_\varphi^2}{r} - u_r \frac{\partial u_r}{\partial r} - u_z \frac{\partial u_r}{\partial z} - \frac{1}{\rho}\frac{\partial p}{\partial r} + \nu\left(\frac{1}{r}\frac{\partial}{\partial r}\left(r\frac{\partial u_r}{\partial r}\right) + \frac{\partial^2 u_r}{\partial z^2} - \frac{u_r}{r^2}\right) - \frac{\Delta^*\Psi}{4\pi^2 r^2 \rho\mu}\frac{\partial \Psi}{\partial r} - \frac{\mu I}{4\pi^2 r^2 \rho}\frac{\partial I}{\partial r} \tag{S3}$$

$$\frac{\partial u_\varphi}{\partial t} = -\frac{u_r u_\varphi}{r} - u_r \frac{\partial u_\varphi}{\partial r} - u_z \frac{\partial u_\varphi}{\partial z} + \nu\left(\frac{1}{r}\frac{\partial}{\partial r}\left(r\frac{\partial u_\varphi}{\partial r}\right) + \frac{\partial^2 u_\varphi}{\partial z^2} - \frac{u_\varphi}{r^2}\right) + \frac{1}{4\pi^2 r^2 \rho}\left(\frac{\partial I}{\partial z}\frac{\partial \Psi}{\partial r} - \frac{\partial I}{\partial r}\frac{\partial \Psi}{\partial z}\right\} \tag{S4}$$

$$\frac{\partial u_z}{\partial t} = -u_r \frac{\partial u_z}{\partial r} - u_z \frac{\partial u_z}{\partial z} - \frac{1}{\rho}\frac{\partial p}{\partial z} + \nu\left(\frac{1}{r}\frac{\partial}{\partial r}\left(r\frac{\partial u_z}{\partial r}\right) + \frac{\partial^2 u_z}{\partial z^2}\right) + g_z - \frac{\Delta^*\Psi}{4\pi^2 r^2 \rho\mu}\frac{\partial \Psi}{\partial z} - \frac{\mu I}{4\pi^2 r^2 \rho}\frac{\partial I}{\partial z} \tag{S5}$$

$$\frac{1}{r}\frac{\partial (r u_r)}{\partial r} + \frac{\partial u_z}{\partial z} = 0 \tag{S6}$$

where $\Delta^* := r\frac{\partial}{\partial r}\frac{1}{r}\frac{\partial}{\partial r} + \frac{\partial^2}{\partial z^2}$ is the Grad-Shafranov operator, where $\nabla := \hat{a}_r \frac{\partial}{\partial r} + \hat{a}_z \frac{\partial}{\partial z}$ is the axisymmetric gradient operator, where ν is kinematic viscosity, ρ is density, σ is conductivity, and μ is permeability.

The spatial boundary conditions for Eq (S1) are the TF coil system's ampere-turns at the exterior of Figure 1's conductor region and $I = I_s$ at the liquid metal's inner plasma-facing free-surface, where I_s is given by

$$I_s = \frac{2\pi}{\mu}\frac{\Phi}{\oint_{\partial S}\frac{z}{r}dr} \tag{S7}$$

EMR performance is partly controlled by the power supply voltage, which affects the boundary condition for Equation (S1). In Eq (S7) the contour integration path is the time-varying free-surface's shape, ∂S (See Figure 6.1), and the enclosed flux variable, $\Phi(t)$, varies over time according to the following ODE:

$$\frac{d\Phi}{dt} = V_{PS} - \frac{1}{2\pi\sigma}\oint_{\partial S}\left(\frac{\partial I}{\partial r}\frac{\partial z}{r} - \frac{\partial I}{\partial z}\frac{\partial r}{r}\right) + \frac{\mu I_s}{2\pi}\oint_{\partial S}\frac{(u_r dz - u_z dr)}{r} + \frac{1}{2\pi}\oint_{\partial S}\frac{u_\varphi}{r}d\Psi \tag{S8}$$

These integrals are also evaluated around the liquid metal's free-surface contour. V_{PS} is the possibly time varying dc control voltage galvanically applied to the liquid metal by the external power supply in Figure 6.1. (Note Eq (8) neglects plasma poloidal current effects, but is exact for a true vacuum region.) The "no-slip" boundary condition, $\vec{u} = 0$, applies to velocity on liquid/solid interfaces. Velocity is unconstrained on the free-surface but the pressure is $p|_{FreeSurface} = \gamma\left(\frac{1}{R_1} + \frac{1}{R2}\right)$ (S9)

where γ is the liquid's surface tension parameter, R_1 , R_2. are local surface curvature radii.

The continuity equation (S6) is replaced by the Pressure Poisson Equation (PPE) whose solution is a pressure field which enforces (S6). The PPE is:

$$\nabla^2 p = -\rho\left(\frac{1}{r}\frac{\partial}{\partial r}\left(r\left[\frac{u_\varphi^2}{r} - u_r\frac{\partial u_r}{\partial r} - u_z\frac{\partial u_r}{\partial z}\right]\right) + \frac{\partial}{\partial z}\left[-u_r\frac{\partial u_z}{\partial r} - u_z\frac{\partial u_z}{\partial z}\right]\right)$$
$$-\frac{1}{4\pi^2 r\rho}\left(\frac{\partial}{\partial r}\left(\frac{1}{r}\left[\frac{\Delta^* \Psi}{\mu}\frac{\partial \Psi}{\partial r} + \mu I\frac{\partial I}{\partial r}\right]\right) + \frac{\partial}{\partial z}\left(\frac{1}{r}\left[\frac{\Delta^* \Psi}{\mu}\frac{\partial \Psi}{\partial z} + \mu I\frac{\partial I}{\partial z}\right]\right)\right) \tag{S10}$$

It should be noted that Equations (S1)-(S10) are not closed because they do not completely describe the poloidal flux boundary conditions on the surfaces of the liquid and solid metallic conductors. These time-varying boundary conditions depend on the plasma and poloidal field coil currents, which depend on the plasma scenario. For the case of no plasma or PF coil currents, the above equations are closed and are ready to be solved for specific cases. For cases including a plasma and/or PF coil current histories, additional data is needed to conduct an analysis. The best approach to providing this data would be to marry the LMMHD simulation with an axisymmetric plasma simulation such as TSC.

Although greatly simplified from the 3-D case, the above equations (S1) through (S10) are not amenable to direct analytical solution unless many approximating

assumptions are made. That has not been done. The equations are amenablet to numerical solution. No commercially available simulation code was identified capable of such a simulation, so one was coded. However, the code's debugging was not complete at the time of this report, so no detailed numerical studies of the EMR concept could be included herein.

In the absence of simulation results, some qualitative observations can be made directly about the equations. They follow:

1. If liquid motion were aligned to poloidal flux surfaces then $u_r \frac{\partial \Psi}{\partial r} + u_z \frac{\partial \Psi}{\partial z} = 0$, which would imply through Eq. (S2) that $\frac{\partial \Psi}{\partial t} = \frac{1}{\sigma\mu}\Delta^* \Psi$. But that simply describes poloidal field diffusion into a stationary axisymmetric conductor (e.g., a solid conductor). We know that this is generally stabilizing or neutral for the plasma, and that its associated toroidal eddy currents decay to zero ($\Delta^* \Psi \rightarrow 0$). Then Equations (S3) and (S5) show that the liquid metal's poloidal velocity becomes independent of poloidal flux.

2. The toroidal swirl motion, $u_\varphi \neq 0$ is characterized by Equation (S4), which predicts that toroidal swirl motion could remain identically zero at all locations and times as long as $\frac{\partial I}{\partial z}\frac{\partial \Psi}{\partial r} - \frac{\partial I}{\partial r}\frac{\partial \Psi}{\partial z} = 0$, i.e., as long as the poloidal current in the liquid metal is aligned with poloidal flux surfaces.

3. For a familiar stationary solid conductor, Equation (S1) becomes $\frac{\partial I}{\partial t} = \frac{1}{\sigma\mu}\Delta^* I$, which describes the diffusion of current into the conductor and its relaxing to its steady-state configuration. For a liquid there are other terms, including :

   a) $u_r \frac{\partial I}{\partial r} + u_z \frac{\partial I}{\partial z}$ which is nonzero where the injected current is misaligned from the velocity, e.g. at current injection electrodes,

   b) $+\frac{2u_r I}{r}$ which generates "diamagnetic drag" in conjunction with Eq.(S3). Note that recasting Eq. S1 by using the variable, $\frac{I}{r^2}$ instead of the variable, I, causes this $+\frac{2u_r I}{r}$ term to be absorbed into the convection terms for "frozen-in" toroidal magnetic flux.

   c) $\nabla\Psi \times \nabla(\frac{u_\varphi}{r})$ which is zero unless a toroidal swirl exists, is nonuniform, and its nonunifomity is misaligned with poloidal flux surfaces.

6.4.4 Simulation Structure

For the special case with no azimuthal (toroidal) swirl motion and no poloidal field, the evolution equations simplify to the following set which has been coded for the initial simulation:

$$\frac{\partial I}{\partial t} = -(u_r)\left(\frac{\partial I}{\partial r}\right) - (u_z)\left(\frac{\partial I}{\partial z}\right) + \frac{1}{\sigma\mu}\left[\left(\frac{\partial^2 I}{\partial r^2}\right) - \frac{1}{r}\left(\frac{\partial I}{\partial r}\right) + \left(\frac{\partial^2 I}{\partial z^2}\right)\right] + \frac{2}{r}(u_r)(I)$$

$$\frac{\partial u_r}{\partial t} = -(u_r)\left(\frac{\partial u_r}{\partial r}\right) - (u_z)\left(\frac{\partial u_r}{\partial z}\right) - \frac{1}{\rho}\left(\frac{\partial p}{\partial r}\right) + \nu\left[\left(\frac{\partial^2 u_r}{\partial r^2}\right) + \frac{1}{r}\left(\frac{\partial u_r}{\partial r}\right) - \frac{1}{r^2}(u_r) + \left(\frac{\partial^2 u_r}{\partial z^2}\right)\right] - \frac{\mu}{4\pi^2\rho r^2}(I)\left(\frac{\partial I}{\partial r}\right)$$

$$\frac{\partial u_z}{\partial t} = -(u_r)\left(\frac{\partial u_z}{\partial r}\right) - (u_z)\left(\frac{\partial u_z}{\partial z}\right) - \frac{1}{\rho}\left(\frac{\partial p}{\partial z}\right) + \nu\left[\left(\frac{\partial^2 u_z}{\partial r^2}\right) + \frac{1}{r}\left(\frac{\partial u_z}{\partial r}\right) + \frac{\partial^2 u_z}{\partial z^2}\right] + g_z - \frac{\mu}{4\pi^2\rho r^2}(I)\left(\frac{\partial I}{\partial z}\right)$$

$$\begin{aligned} 0 = & -\frac{1}{\rho}\frac{\partial}{\partial r}\left(\frac{\partial p}{\partial r}\right) - \frac{1}{\rho r}\left(\frac{\partial p}{\partial r}\right) - \frac{1}{\rho}\frac{\partial}{\partial z}\left(\frac{\partial p}{\partial z}\right) \\ & - \frac{1}{r}(u_r)\left(\frac{\partial u_r}{\partial r}\right) - \frac{1}{r}(u_z)\left(\frac{\partial u_r}{\partial z}\right) - \left(\frac{\partial u_r}{\partial r}\right)^2 - 2\left(\frac{\partial u_z}{\partial r}\right)\left(\frac{\partial u_r}{\partial z}\right) \\ & - \left(\frac{\partial u_z}{\partial z}\right)^2 - (u_r)\left(\frac{\partial^2 u_r}{\partial r^2}\right) - (u_z)\left(\frac{\partial^2 u_r}{\partial r \partial z}\right) - (u_r)\left(\frac{\partial^2 u_z}{\partial r \partial z}\right) - (u_z)\left(\frac{\partial^2 u_z}{\partial z^2}\right) \\ & - \frac{\mu}{4\pi^2\rho r^2}\left\{(I)\left[\left(\frac{\partial^2 I}{\partial r^2}\right) - \frac{1}{r}\left(\frac{\partial I}{\partial r}\right) + \left(\frac{\partial^2 I}{\partial z^2}\right)\right] + \left(\frac{\partial I}{\partial r}\right)^2 + \left(\frac{\partial I}{\partial z}\right)^2\right\} \end{aligned}$$

An adaptive unstructured grid is used in the simulation both to track the free surface boundary and also to resolve internal boundary layers without requiring an excessive number of grid points. The free surface boundary nodes are moved within each time step, following the free surface motion. Internal nodes are then reallocated, repositioned , and interpolated between time steps.

In order to avoid intolerable complexity in the algorithm for moving free surface boundary nodes, the finite elements adjacent to the free surface must have a simple structure. In particular, complicated finite elements with internal nodes not on the free

surface boundary and with associated higher order interpolation functions would require more sophisticated algorithms to implement free surface boundary motion than needed for piecewise linear interpolation on triangular cross section finite elements. To simplify the simulation, simple axisymmetric ring elements with triangular cross section and piecewise-linear C^0 continuity interpolation are used for all field variables throughout the computational domain.

Published literature documents various unsuccessful experiences in computing solutions to Navier-Stokes equations for incompressible fluid flow using Galerkin finite element formulations, with some reported problems being quite subtle. The most common Galerkin formulations include an integration by parts invoking Greens theorem, after which the pressure term enters the formulas directly but only the first spatial derivatives of the velocity terms are included. "Spurious pressure modes" in the solution can result if the same degree of interpolating polynomials is used for both pressure and velocity; it is reported that they can be avoided by using a velocity interpolation polynomial of one higher degree than the polynomial used for pressure interpolation. It is also reported that "spurious pressure modes" are avoided by using an explicit "pressure projection" method, or by using the "least squares" finite element formulation instead of the Galerkin one. Another observed problem is "locking" which prevents finding a nonzero solution when an insufficiently rich set of interpolation functions for velocity are overconstrained by incompressible continuity requirements. "Locking" can also be grid-dependent, with the solutions found on coarse grids not converging as the grid is refined. Quadratic or cubic polynomial interpolation functions for velocity components have been successfully employed in computer codes avoiding both of these pathologies.

This simulation attempts to avoid such numerical difficulties while still using C^0 continuous piecewise linear interpolation for all fields, by using an unconventional Galerkin formulation for velocity and pressure in which Greens theorem is not invoked. Instead of integrating by parts to replace second derivatives by first derivatives, additional simulation variables are employed to separately estimate the first derivatives of the field variables with their own piecewise linear interpolation. Thus, in this formulation, spatial derivatives of the estimated field variables are different from estimates of the field variables' spatial derivatives. This general formulation was termed "Mixed Finite Element Approximation" by Lapidus and Pinder, but no references have been found documenting its performance track record with Navier-Stokes systems.

The unstructured grid used in the simulation is defined by a list of arbitrarily located (r_j,z_j) points, with flags identifying boundary vs. internal subregion points. The grid is Delauney triangulated via a quick version of Bowyer's algorithm implemented with quadtrees and linked list data structures. All functions of (r,z) are approximated on this grid using piecewise-linear pyramidal shape functions, $\varphi_j(r,z)$, one for each grid point. Each shape function equals 1 at its own gridpoint, 0 at all other gridpoints, and varies linearly on each triangle connecting gridpoints. An arbitrary function f(r,z) is approximated as $\hat{F}(r,z) = \sum_j F_j \hat{\varphi}_j(r,z)$ where the coefficients F_j are selected to make the

residual orthogonal in the Galerkin sense to each shape function, i.e. $\left(\hat{\varphi}_j,(\hat{F}-f)\right)=0$ for every i. This can be rewritten as the vector-matrix equation, AF=b where values of $b_i=\int f(r,z)\hat{\varphi}_i(r,z)rdrdz$ can be calculated e.g. by numerical integration and stored in the points list, and where nonzero values of $a_{ij}=\int f(r,z)\hat{\varphi}_i\hat{\varphi}_j rdrdz$ are evaluated from formulas using triangle vertex coordinates and stored in data structures for triangle edges or for points. F is then calculated iteratively, typically converging to less than 1% error within 10 damped Jacobi iterations.

A derivative of an interpolated function, e.g. $\frac{\partial\hat{F}}{\partial z}$, is discontinuous and so cannot itself be differentiated further. However, it can be approximated by a continuous interpolated function, $\hat{H}(r,z)=\sum_j H_j\hat{\varphi}_j(r,z)$ with $\left(\hat{\varphi}_j,(\sum_j F_j\frac{\partial\hat{\varphi}_j}{\partial z}-\sum_j H_j\hat{\varphi}_j(r,z))\right)=0$. This can be written in vector-matrix form as AH=EF for the z-derivative, or AH=CF for the radial derivative. This algorithm and its subsequent relaxation solution is a heavily used part of the simulation code. The nonzero coefficients of A, C, and E are calculated via simple formulas using point coordinates, and stored in the points and edge lists.

The simulation starts each time-step's algorithms by using the stored functions, I, u_r, u_z to calculate $\left(\frac{\partial I}{\partial r}\right),\left(\frac{\partial u_r}{\partial r}\right),\left(\frac{\partial u_z}{\partial r}\right),\left(\frac{\partial I}{\partial z}\right),\left(\frac{\partial u_r}{\partial z}\right),\left(\frac{\partial u_z}{\partial z}\right)$ and then uses these derivatives to calculate, $\left(\frac{\partial^2 I}{\partial r^2}\right),\left(\frac{\partial^2 u_r}{\partial r^2}\right),\left(\frac{\partial^2 u_z}{\partial r^2}\right),\left(\frac{\partial I^2}{\partial z^2}\right),\left(\frac{\partial u_r{}^2}{\partial z^2}\right),\left(\frac{\partial u_z{}^2}{\partial z^2}\right)$, all as piecewise-continuous functions. Then linear interpolates are formed to continuously approximate the right hand side of the evolution equation for I, and then used with explicit Euler integration to determine the later value of I at each interior point.

Similarly, the right hand sides of the Navier Stokes equations are calculated excepting their pressure gradient terms. A provisional new velocity field is formed by explicit Euler integration, but it does not satisfy the continuity condition. The divergence of theprovisional velocity field is then evaluated using the Galerkin gradient algorithm, and the PPE equation is solved by damped Jacobi iteration with a multigrid accelerator. The gradient of the resulting pressure field is then used to "project out" the provisional velocity field's the nonzero divergence and calculate the corrected new velocity field. Its divergence is calculated to be the PPE equations' right hand side. After PPE solution, the pressure field gradient is calculated and used to correct the velocity field at nonconstrained points.

Free surface boundary nodes are movedat the end of each integration time step to track free surface motion. The free surface grid velocity is the component of velocity perpendicular to the free surface. Time step duration is restricted so that total boundary motion is smaller than triangular element size.

Internal nodes are reallocated, retired, or repositioned between time steps by an adaptive point migration algorithm intended to increase accuracy in resolving small features. The modified grid is retriangulated. new grid is retriangulated. Computed point variables are then reinterpolated so that the new field closely matches the old one.

6.5 Electromagnetic Interactions with Tokamak Plasma

The equations of the previous sections include all MHD interactions with an axisymmetric plasma, except for galvanic halo currents flowing between the plasma and the conducting surface, which are not predicted by these equations. There will be causal inteactions in both directions between the plasma's magnetics and the lithium blanket's magnetics, which ideally would necessitate integrated analyses. The choice of variables, I and Ψ, matches the magnetic variables typically used in plasma simulations, and was chosen to simplify the later task of marrying a plasma simulation code with an EMR blanket model.

6.6 Necessary Departures from Axisymmetry

It is not possible to design an entirely axisymmetric blanket system since the flowing liquid must cross between structural supports at some location, and in most versions of the concept need to exit and reenter the TF coil region. Analyses of these nonaxisymmetric regions will be more complex. There may be significant MHD pressure losses and pumping problems in the nonaxisymmetric regions.

6.7 Key Issues and R&D.

The key issues with the EMR Lithium Blanket concept all are based on the difficulty of predicting its performance. At the present time, there are no computer tools or other methods to design such a system. At this time, the key issues are all associated with developing methods to predict how it and variations of it would behave, and experiments with the goal of benchmarking those methods.